J|A|C|S
ARTICLES
Published on Web 12/04/2002

Syntheses, Crystallographic/Computational Characterizations, and Reactions of the First 10-Vertex *arachno*- and *nido*-Phosphamonocarbaboranes

Alexandra M. Shedlow, Daniel E. Kadlecek, Jude C. Clapper, Scott E. Rathmill, Patrick J. Carroll, and Larry G. Sneddon*

Contribution from the Department of Chemistry, University of Pennsylvania, Philadelphia, Pennsylvania 19104-6323

Received July 9, 2002

Abstract: A synthetic sequence involving the initial reaction of a substituted phosphorus dihalide ($RPCl_2$, R = CH_3, C_6H_5) with the *arachno*-$CB_8H_{13}^-$ (**1**$^-$) monoanion followed by an in situ dehydrohalogenation reaction initiated by Proton Sponge, resulted in phosphorus cage insertion to yield the first 10-vertex *arachno*- and *nido*-phosphamonocarbaboranes, *exo*-6-R-*arachno*-6,7-PCB_8H_{12} (**2a**, **2b**) and PSH^+6-R-*nido*-6,9-$PCB_8H_9^-$ (**PSH$^+$3a**$^-$, **PSH$^+$3b**$^-$) (R = C_6H_5 (**a**), CH_3 (**b**)). Alternatively, **2a** and **2b** were synthesized in high yield as the sole product of the reaction of the *arachno*-4-$CB_8H_{12}^{2-}$ (**1^{2-}**) dianion with $RPCl_2$. Crystallographic determinations of **PSH$^+$3a**$^-$ and **PSH$^+$3b**$^-$ in conjunction with DFT/GIAO computational studies of the anions have confirmed the expected nido cage framework based on an octadecahedron missing the six-coordinate vertex. DFT/GIAO computational studies have also shown that while the gross cage geometries of the *exo*-6-R-*arachno*-6,7-PCB_8H_{12} compounds **2a** and **2b** resemble the known isoelectronic *arachno*-6,9-SCB_8H_{12}, the phosphorus and carbon atoms are in thermodynamically unfavorable adjacent positions on the six-membered puckered face. They also each have an *endo*-hydrogen at the P6-position arising from proton transfer to the basic phosphorus during the cage-insertion reaction. Possible stepwise reaction pathways that can account for the formation of both the arachno and nido products are discussed. Deprotonation of **2a** and **2b** resulted in the formation of their corresponding conjugate monoanions, 6-R-*arachno*-6,7-$PCB_8H_{11}^-$ (**2a**$^-$, **2b**$^-$), in which the proton that had been attached to the P6 atom was removed. Reactions of **2a**$^-$ with O_2, S_8, BH_3·THF, or Br_2 further demonstrated the basicity of the P6-phosphorus yielding the new arachno-substituted compounds, *endo*-6-O-*exo*-6-(C_6H_5)-*arachno*-6,7-$PCB_8H_{11}^-$ (**4a**$^-$), *endo*-6-S-*exo*-6-(C_6H_5)-*arachno*-6,7-$PCB_8H_{11}^-$ (**5a**$^-$), *endo*-6-BH_3-*exo*-6-(C_6H_5)-*arachno*-6,7-$PCB_8H_{11}^-$ (**6a**$^-$), and *endo*-6-Br-*exo*-6-(C_6H_5)-*arachno*-6,7-PCB_8H_{11} (**7a**), respectively, in which the O, S, BH_3, and Br substituents are bound to the phosphorus at the endo position.

Introduction

We recently reported high-yield routes for heteroatom-cage insertions into polyborane clusters that have allowed the systematic syntheses of a range of thia- and phospha-boranes, thia- and phospha-dicarbaboranes, and the first thiaphosphaborane cluster.[1,2] We describe here the rational high-yield syntheses of the first 10-vertex *arachno*- and *nido*-phosphamonocarbaboranes,[3] *exo*-6-R-*arachno*-6,7-PCB_8H_{12}, and 6-R-*nido*-6,9-$PCB_8H_9^-$ along with their structural characterizations using combined crystallographic and DFT/GIAO/NMR methods. We also report systematic studies of the reactions of the *exo*-6-R-*arachno*-6,7-$PCB_8H_{11}^-$ anion with Lewis acids that have demonstrated that this anion, in contrast to the other known phosphaborane clusters, exhibits strong donor properties arising from an electron lone pair localized on the phosphorus. We further demonstrate in the following paper, that these 10-vertex phosphamonocarboranes are an important new class of highly versatile cluster ligands that can stabilize transition metals in an unprecedented variety of coordination geometries and formal oxidation states.[4]

Experimental Section

All manipulations were carried out using standard high-vacuum or inert-atmosphere techniques as described by Shriver.[5]

Materials. Proton Sponge (1,8-bis(dimethylamino)naphthalene, PS), BH_3·THF (1.0 M solution in THF), HCl·OEt_2 dichlorophenylphosphine, and dichloromethylphosphine were purchased from Aldrich and used as received. Bromine was purchased from Alfa Aesar and used as received. Oil-dispersed sodium hydride was purchased from Aldrich, washed with dry hexanes under a N_2 atmosphere, and then dried under vacuum. Tetrahydrofuran was dried over sodium/benzophenone ketyl

* Address correspondence to this author. E-mail: lsneddon@sas.upenn.edu.

(1) Shedlow, A. M.; Sneddon, L. G. *Inorg. Chem.* **1998**, *37*, 5269−5277.
(2) Hong, D.; Rathmill, S. E.; Kadlecek, D. E.; Sneddon, L. G. *Inorg. Chem.* **2000**, *39*, 4996−4997.
(3) The first 10-vertex *closo*-phosphamonocarboranes were recently reported, see: Holub, J.; Bakardjiev, M.; Stíbr, B.; Hnyk, D.; Tok, O. L.; Wrackmeyer, B. *Inorg. Chem.* **2002**, *41*, 2817−2819.
(4) Kadlecek, D. E.; Shedlow, A. M.; Kang, S. O.; Carroll, P. J.; Sneddon, L. G. *J. Am. Chem. Soc.* **2002**, *124*, 212−220.
(5) Shriver, D. F.; Drezdzon, M. A. *Manipulation of Air-Sensitive Compounds*, 2nd ed.; Wiley: New York, 1986.

10.1021/ja020944j CCC: $25.00

and distilled prior to use. Anhydrous diethyl ether was purchased from Fisher and used as received. The *arachno*-4-CB_8H_{14} was prepared according to the literature procedure.[6]

Physical Measurements. ^{1}H NMR spectra at 500.4 MHz, ^{11}B NMR spectra at 160.5 MHz, ^{13}C NMR at 125.8 MHz, and ^{31}P NMR spectra at 202.6 MHz were obtained on a Bruker AM-500 spectrometer equipped with the appropriate decoupling accessories. The ^{11}B NMR at 64.2 MHz and ^{1}H NMR at 200 MHz were obtained on a Bruker AC-200 spectrometer. The ^{31}P NMR spectra at 145.8 MHz were obtained on a Bruker AM-360 spectrometer. All ^{11}B chemical shifts are referenced to external $BF_3{\cdot}O(C_2H_5)_2$ (0.00 ppm) with a negative sign indicating an upfield shift. All ^{1}H and ^{13}C chemical shifts were measured relative to internal residual protons or carbons in the lock solvent and are referenced to Me_4Si (0.00 ppm). All ^{31}P chemical shifts are referenced to external 85% H_3PO_4 (0.0 ppm) with a negative sign indicating an upfield shift. Two-dimensional COSY ^{11}B-^{11}B NMR experiments and two-dimensional HETCORR ^{11}B-^{1}H experiments were performed at 160.5 MHz using the procedures described previously.[7] High- and low-resolution mass spectra (HRMS and LRMS) were recorded on a Micromass Autospec spectrometer. Infrared spectra were recorded on a Perkin-Elmer 1430 spectrophotometer. FT and diffuse-reflectance (DRIFT) infrared spectra were obtained on a Perkin-Elmer System 2000 FTIR spectrophotometer. Elemental analyses were performed at the University of Pennsylvania microanalysis facility. Melting points were obtained on a standard melting point apparatus and are uncorrected.

Synthesis of *exo*-6-(C_6H_5)-*arachno*-6,7-PCB_8H_{12} (2a) and PSH^+6-(C_6H_5)-*nido*-6,9-$PCB_8H_9^-$ (PSH^+3a$^-$) from *arachno*-4-$CB_8H_{13}^-$ (1^-). To a 250-mL, two-neck, round-bottom flask fitted with a vacuum adapter, magnetic stirbar, and septum was added 1.13 g (10.0 mmol) of *arachno*-4-CB_8H_{14} (**1**). The flask was then attached to the high-vacuum line and 100 mL of dry THF was condensed into the flask at −196 °C. The flask was then attached to the Schlenk line and, after equilibrating the solution at 0 °C, 4.3 g (20.0 mmol) of Proton Sponge was added through one neck of the flask under a N_2 flow. Then, 1.80 g (10.1 mmol) of dichlorophenylphosphine was added dropwise via syringe. The solution was then stirred for 3 h at which point ^{11}B NMR analysis indicated nearly quantitative formation of *exo*-6-(C_6H_5)-*arachno*-6,7-PCB_8H_{12} (**2a**). The solution was then taken into the glovebag, filtered, and the volatiles removed from the filtrate under reduced pressure. Extraction of the yellow residue with 5 × 50 mL portions of diethyl ether followed by concentration of the combined extracts under reduced pressure and drying of the residue overnight under high-vacuum afforded 2.1 g (9.6 mmol, 96%) of *exo*-6-(C_6H_5)-*arachno*-6,7-PCB_8H_{12} (**2a**): yellow, oily solid; mp 76 °C (dec); anal. calcd for $C_7H_{17}B_8P$: C, 38.45; H, 7.84; found C, 38.39; H, 7.76; HRMS calcd for $^{12}C_7{}^1H_{17}{}^{11}B_8{}^{31}P_1$ (P) *m*/*e* 220.1812; found *m*/*e* 220.1800; DRIFT (KBr, cm^{-1}): 3225 (w), 3043 (s), 3032 (s), 2622 (s), 2578 (vs), 2516 (s), 2250 (s), 1965 (w), 1897 (w), 1812 (w), 1586 (m), 1484 (m), 1437 (s), 1313 (m), 1186 (w), 1137 (w), 1111 (m), 1028 (w), 985 (w), 952 (m), 854 (m), 739 (m), 690 (m), 611 (s), 517 (s), 425 (m, br). The compound was normally stored as a ∼0.15 M stock solution, which was prepared by dissolving the oily solid in an appropriate amount of dry THF.

The yellow solid remaining after the diethyl ether extractions was collected to give 0.1 g (0.23 mmol, 2.3%) of PSH^+6-(C_6H_5)-*nido*-6,9-$PCB_8H_9^-$ (PSH^+3a$^-$). Elemental analysis was performed on solid PSH^+3a$^-$ obtained from recrystallization in CH_2Cl_2/hexanes. Anal. calcd for $[PSH^+6\text{-}(C_6H_5)\text{-}nido\text{-}6,9\text{-}PCB_8H_9^-]_{1.00}[CH_2Cl_2]_{0.77}$: C, 52.68; H, 7.01; N, 5.64; found: C, 52.64; H, 7.33; N, 5.51; IR (KBr plates, CCl_4, cm^{-1}): 3210 (s), 2510 (s), 1390 (s), 1310 (m), 1020 (w), 930 (w).

Synthesis of *exo*-6-CH_3-*arachno*-6,7-PCB_8H_{12} (2b) and PSH^+6-CH_3-*nido*-6,9-$PCB_8H_9^-$ (PSH^+3b$^-$) from *arachno*-4-$CB_8H_{13}^-$ (1^-). A 0.225-g (2.0 mmol) sample of **1** was dissolved in 40 mL of dry THF under a N_2 atmosphere. To this stirred solution was added 1.07 g (5.0 mmol) of Proton Sponge. Then, 0.18 mL (2.0 mmol) of dichloromethylphosphine was injected dropwise at room temperature. After 18 h, the solution was filtered to remove PSH^+Cl^-. The solvent was removed under reduced pressure and the oily residue extracted with toluene. The toluene was then vacuum evaporated and the resulting yellow solid was dried under vacuum to give 0.294 g (1.88 mmol, 94.0% yield) of *exo*-6-CH_3-*arachno*-6,7-PCB_8H_{12} (**2b**) as a pale yellow solid. For **2b**: Anal. calcd for $C_2H_{15}B_8P_1$: C, 15.34; H, 9.65; found: C, 15.17; H, 9.45; HRMS calcd for $^{12}C_2{}^1H_{15}{}^{11}B_8{}^{31}P_1$ *m*/*e* 158.1656; found, 158.1648; mp 140−141 °C (dec); IR (NaCl, CH_2Cl_2, cm^{-1}): 3231 (w), 3050 (s), 2600 (s), 2560 (vs), 2541 (s), 2360 (s), 2260 (s), 1471 (m), 1438 (s), 1419 (m), 1395 (m), 1310 (m), 1194 (w), 1110 (m), 1015 (w), 930 (m), 836 (m), 776 (m), 738 (m), 682 (m), 645 (s), 543 (s), 484 (m, br).

Only very small amounts of PSH^+3b$^-$ were observed to have been formed in reactions carried out with the conditions described above. However, when the reactions were carried out with twice the concentration of **1** and at lower temperatures, higher yields of PSH^+3b$^-$ were obtained. Thus, in a typical reaction, 0.225 g (2.0 mmol) of **1**, dissolved in 20 mL of dry THF, was reacted at 0 °C with 1.07 g (5.0 mmol) of Proton Sponge, followed by the dropwise addition of 0.18 mL (2.0 mmol) of dichloromethylphosphine. The mixture was then allowed to stir for 1 h at which time ^{11}B NMR analysis of the reaction mixture indicated nearly quantitative formation of PSH^+6-CH_3-*nido*-6,9-$PCB_8H_9^-$ (PSH^+3b$^-$). The reaction mixture was filtered in the glovebag to remove precipitated PSH^+Cl^- and the resulting solid washed with 2 × 20 mL portions of dry THF. Drying of the solid overnight under high vacuum afforded an oily yellow solid. This solid was then extracted with 4 × 20 mL portions of toluene, followed by 4 × 20 mL portions of diethyl ether until a bright, yellow powder resulted. The product was then dried under high vacuum to yield 0.679 g (1.84 mmol, 92%) of PSH^+6-CH_3-*nido*-6,9-$PCB_8H_9^-$ (PSH^+3b$^-$). For PSH^+3b$^-$: Anal. calcd for $C_{16}H_{31}N_2B_8P_1$: C, 52.10; H, 8.47; N, 7.59; found: C, 52.07; H, 8.42; N, 7.60; mp 265−267 °C (dec); IR (NaCl, CH_2Cl_2, cm^{-1}): 3520 (w), 3225 (s), 3045 (w), 2960 (s), 2860 (w), 2500 (vs), 2350 (w), 1595 (m), 1509 (m), 1452 (m), 1402 (m), 1295 (w), 1260 (m), 1216 (m), 1155 (w), 1100 (w), 1030 (m), 900 (m), 825 (w), 764 (m), 728 (s).

Synthesis of *exo*-6-R-*arachno*-6,7-PCB_8H_{12} (2a and 2b) from *arachno*-4-$CB_8H_{12}^{2-}$ (1^{2-}). To a 250-mL, two-neck, round-bottom flask fitted with a vacuum adapter, magnetic stirbar, and septum was added 0.79 g (7.0 mmol) of **1** under a flow of N_2. Approximately 40 mL of THF was added by vacuum transfer. The stirring solution was maintained at 0 °C while 0.49 g (21.0 mmol) of NaH was added. After 30 min, ^{11}B NMR analysis of the reaction mixture indicated complete formation of *arachno*-4-$CB_8H_{12}^{2-}$ (1^{2-}).[8] The solution was then taken into the glovebag and filtered to remove excess NaH. After reattaching the flask to the Schlenk line, the stirring solution was maintained at 0 °C, while 1.3 g (7.0 mmol) of dichlorophenylphosphine was added dropwise via syringe. ^{11}B NMR analysis of the reaction mixture after 12 h indicated the exclusive formation of *exo*-6-(C_6H_5)-*arachno*-6,7-PCB_8H_{12} (**2a**). The reaction was then filtered in the glovebag and the THF removed from the filtrate under reduced pressure to give 1.45 g (6.6 mmol, 94% yield) of **2a**.

An analogous reaction of 0.226 g (2.0 mmol) of **1**, excess NaH and 0.24 mL (2.0 mmol) of dichloromethylphosphine yielded 0.253 g (1.6 mmol, 80% yield) of *exo*-6-CH_3-*arachno*-6,7-PCB_8H_{12} (**2b**).

Synthesis of *exo*-6-R-*arachno*-6,7-$PCB_8H_{11}^-$ (2a$^-$ and 2b$^-$) from *exo*-6-R-*arachno*-6,7-PCB_8H_{12} (2a and 2b). To a 100-mL, two-neck, round-bottom flask fitted with a vacuum adapter, magnetic stirbar, and

(6) Wille, A. E.; Plesek, J.; Holub, J.; Stíbr, B.; Carroll, P. J.; Sneddon, L. G. *Inorg. Chem.* **1996**, *35*, 5342−5346.
(7) Kang, S. O.; Carroll, P. J.; Sneddon, L. G. *Organometallics* **1988**, *7*, 772−776.
(8) Kadlecek, D. E.; Sneddon, L. G. *Inorg. Chem.* **2002**, *41*, 4239−4244.

septum was added under a flow of N_2 a solution of 0.604 g (2.76 mmol) of **2a** in diethyl ether. An excess of Proton Sponge (or LiH or NaH) in diethyl ether was then added to the flask. After 30 min, NMR analysis of the reaction mixture indicated complete formation of the air-sensitive salt *exo*-6-(C_6H_5)-*arachno*-6,7-$PCB_8H_{11}^-$ (**PSH$^+$2a$^-$**).

An analogous reaction of 0.156 g (1.0 mmol) of **2b** and 0.214 g (1.0 mmol) of Proton Sponge in THF afforded the air-sensitive salt, *exo*-6-CH_3-*arachno*-6,7-$PCB_8H_{11}^-$ (**PSH$^+$2b$^-$**).

Reprotonation of a 0.109-g (0.5 mmol) sample of **Na$^+$2a$^-$** (prepared from the reaction of NaH and **2a**) in diethyl ether with 1.0 mmol of HCl·OEt_2 resulted in the regeneration of **2a**.

Synthesis of *endo*-6-O-*exo*-6-R-*arachno*-6,7-$PCB_8H_{11}^-$ (4a$^-$). To a 50-mL, two-neck, round-bottom flask fitted with a vacuum adapter, magnetic stirbar, and septum was added via syringe 5.0 mL (1.0 mmol) of a 0.20 M solution of *exo*-6-(C_6H_5)-*arachno*-6,7-PCB_8H_{12} (**2a**) in THF. After cooling the solution to 0 °C, 0.214 g (1.0 mmol) of Proton Sponge was added through one neck of the flask to generate **PSH$^+$2a$^-$**. Once the reaction was determined to be complete by ^{11}B NMR, the solution was opened to the air. Within several minutes, the ^{11}B NMR indicated that complete conversion to the new anion **4a$^-$** had occurred. The volatiles were then removed under reduced pressure to leave an oily, light yellow solid. The oily solid was then precipitated from THF/pentane to afford 0.408 g (0.91 mmol, 91%) of PSH$^+$*endo*-6-O-*exo*-6-(C_6H_5)-*arachno*-6,7-$PCB_8H_{11}^-$ (**PSH$^+$4a$^-$**). For **4a$^-$**: HRMS calcd for $^{12}C_7{}^1H_{16}{}^{11}B_8{}^{31}P_1{}^{16}O_1$ *m*/*e* 235.1683; found, 235.1693; IR (NaCl plates, CH_2Cl_2, cm^{-1}): 2525 (vs), 2390 (w), 1450 (m), 1409 (s), 1300 (s), 1021 (m), 920 (m), 825 (w), 725 (s), 705(m).

Synthesis of *endo*-6-S-*exo*-6-R-*arachno*-6,7-$PCB_8H_{11}^-$ (5a$^-$). To a 100-mL, three-neck, round-bottom flask fitted with a vacuum adapter, magnetic stirbar, septum, and sidearm addition tube containing 0.048 g (1.5 mmol) of elemental sulfur was added via syringe 8.3 mL (1.0 mmol) of a 0.12 M solution of *exo*-6-(C_6H_5)-*arachno*-6,7-PCB_8H_{12} (**2a**) in THF. The volatiles were then vacuum evaporated to leave an oily, yellow solid. A solution of 0.214 g (1.0 mmol) of Proton Sponge in 20 mL of $CHCl_3$ was then added to generate **PSH$^+$2a$^-$**. After cooling the solution to 0 °C, the elemental sulfur was added by tipping the sidearm attachment. Within several minutes, ^{11}B NMR indicated that complete conversion to the new compound (**5a$^-$**) had occurred. The solution was filtered and the volatiles were removed under reduced pressure to leave an oily residue, which was extracted with THF. The THF was then removed in vacuo to leave an oily, light yellow solid. The solid was recrystallized from THF/pentane to afford 0.414 g (0.89 mmol, 89%) of PSH$^+$*endo*-6-S-*exo*-6-(C_6H_5)-*arachno*-6,7-$PCB_8H_{11}^-$ (**PSH$^+$5a$^-$**). For **5a$^-$**: Anal. calcd for $(C_{21}H_{35}N_2B_8P_1S_1)_{1.00}$ $(THF)_{0.90}$: C, 55.77; H, 8.03; N, 5.28; found: C, 55.38; H, 8.04; N, 4.88; HRMS calcd for $^{12}C_7{}^1H_{16}{}^{11}B_8{}^{31}P_1{}^{32}S_1$ *m*/*e* 251.1455; found, 251.1465; IR (NaCl plates, CH_2Cl_2, cm^{-1}): 3300 (m), 2530 (vs), 1605 (w), 1458 (m), 1435 (m), 1220 (w), 1160 (w), 1100 (w), 1027 (m), 945 (w), 825 (m), 809 (w), 729 (s), 695 (s).

Synthesis of *endo*-6-BH_3-*exo*-6-(C_6H_5)-*arachno*-6,7-$PCB_8H_{11}^-$ (6a$^-$). To a 100-mL, two-neck, round-bottom flask fitted with a vacuum adapter, magnetic stirbar, and septum was added via syringe 4.3 mL (1.0 mmol) of a 0.23 M solution of *exo*-6-(C_6H_5)-*arachno*-6,7-PCB_8H_{12} (**2a**) in THF. After cooling the solution to 0 °C, 0.21 g (1.0 mmol) of Proton Sponge was added through one neck of the flask to generate **PSH$^+$2a$^-$**. Then, 1.5 mL (1.5 mmol) of 1.0 M BH_3·THF was added dropwise via syringe. After stirring for 2 h, ^{11}B NMR analysis of the reaction mixture indicated near quantitative formation of PSH$^+$*endo*-6-BH_3-*exo*-6-(C_6H_5)-*arachno*-6,7-$PCB_8H_{11}^-$ (**PSH$^+$6a$^-$**). The volatiles were then removed under reduced pressure and the resulting oily solid washed with diethyl ether to afford 0.23 g (0.51 mmol, 51%) of PSH$^+$*endo*-6-BH_3-*exo*-6-(C_6H_5)-*arachno*-6,7-$PCB_8H_{11}^-$ (**PSH$^+$6a$^-$**) as a pale yellow solid. IR (NaCl, CCl_4, cm^{-1}): 2500 (vs), 2390 (s), 2305 (s), 1450 (s), 1430 (s), 1410 (w), 1405 (w), 1375 (m), 1265 (w), 1220 (m), 1180 (w), 1150 (w), 1090 (w), 1030 (s), 1010 (w), 940 (m), 890 (w), 690 (m), 605 (w), 580 (m), 490 (m), 460 (m).

Synthesis of *endo*-6-Br-*exo*-6-(C_6H_5)-*arachno*-6,7-PCB_8H_{11} (7a). To a 100-mL, two-neck, round-bottom flask fitted with a vacuum adapter, magnetic stirbar, and septum was added, via syringe, 6.1 mL (1.0 mmol) of a 0.16 M solution of **2a** in THF. After cooling the solution to 0 °C, 0.21 g (1.0 mmol) of Proton Sponge was added through one neck of the flask under a N_2 flow to generate PSH$^+$6-(C_6H_5)-*arachno*-6,7-$PCB_8H_{11}^-$ (**PSH$^+$2a$^-$**). With the solution at 0 °C, 0.05 mL (1.0 mmol) of bromine was added dropwise via syringe. After stirring for 1 h, ^{11}B NMR analysis of the reaction mixture indicated near quantitative formation of *endo*-6-Br-*exo*-6-(C_6H_5)-*arachno*-6,7-PCB_8H_{11} (**7a**). The reaction was filtered in the glovebag to remove the precipitated PSH$^+$Br$^-$ and the filtrate then concentrated under reduced pressure to afford a yellow residue. The residue was then extracted with diethyl ether and the volatiles removed from the combined extracts under reduced pressure. The resulting oil was sublimed at 60 °C under vacuum to yield 0.14 g (0.47 mmol, 47%) of *endo*-6-Br-*exo*-6-(C_6H_5)-*arachno*-6,7-PCB_8H_{11} (**7a**) as a pale yellow oil. LRMS (CI-) (*m*/*e*) calcd for $^{12}C_7{}^{11}B_8{}^1H_{16}{}^{31}P_1{}^{81}Br_1$: 300, found 300 with the peaks in the parent envelope having relative intensities in accord with the expected isotopic composition.

Crystallographic Data for PSH$^+$3a$^-$ (Upenn #3149), PSH$^+$3b$^-$ (Upenn #3158), and PSH$^+$5a$^-$ (Upenn #3201). Yellow crystals of both **PSH$^+$3a$^-$** and **PSH$^+$3b$^-$** were grown from hexanes/CH_2Cl_2 solutions of the compounds at −25 °C inside a glovebox. Clear crystals of **PSH$^+$5a$^-$** were grown from pentane/THF solutions at −10 °C inside a refrigerator.

Collection and Reduction of the Data. X-ray intensity data for **PSH$^+$3a$^-$** and **PSH$^+$3b$^-$** were collected on a Rigaku R-AXIS IIc area detector employing graphite-monochromated Mo−K_α radiation at a temperature of 200 K for **PSH$^+$3a$^-$** and 210 K for **PSH$^+$3b$^-$**. X-ray intensity data for **PSH$^+$5a$^-$** were collected on a Rigaku Mercury CCD area detector employing graphite-monochromated Mo−K_α radiation at a temperature of 143 K. Indexing for **PSH$^+$3a$^-$** and **PSH$^+$3b$^-$** was performed from a series of 1° oscillation images with exposures of 4 min per frame for **PSH$^+$3a$^-$** and 5 min per frame for **PSH$^+$3b$^-$**. A hemisphere of data was collected using 5° oscillation angles with exposures of 5 min per frame for **PSH$^+$3a$^-$** and 500 s for **PSH$^+$3b$^-$** at a crystal-to-detector distance of 82 mm. Indexing for **PSH$^+$5a$^-$** was performed from a series of four 0.5° oscillation images with exposures of 20 s per frame. A hemisphere of data was collected using 30 s exposures and a crystal-to-detector distance of 35 mm. Oscillation images were processed using bioteX[9] (**PSH$^+$3a$^-$** and **PSH$^+$3b$^-$**) or CrystalClear[10] (**PSH$^+$5a$^-$**) producing a listing of unaveraged F^2 and $\sigma(F^2)$ values which were then passed to the teXsan[11] program package for further processing and structure solution on Silicon Graphics Indigo R4000 or O2 computers. The intensity data were corrected for Lorentz and polarization effects. The intensity data for **PSH$^+$5a$^-$** were also corrected for absorption using REQAB[12] (minimum and maximum transmission 0.720, 1.000).

Solution and Refinement of the Structure. The structures were solved by direct methods (SIR92).[13] Refinement was by full-matrix least squares based on F^2 using SHELXL-93.[14] All reflections were used during refinement (F^2's that were experimentally negative were replaced by $F^2 = 0$). The weighting scheme used was $w = 1/[\sigma^2(F_o^2) + aP^2 + bP]$ where $P = (F_o^2 + 2F_c^2)/3$. Non-hydrogen atoms were refined anisotropically and hydrogen atoms were refined isotropically, except for the THF hydrogen atoms in the structure of **PSH$^+$5a$^-$** which were instead refined using a "riding" model.

(9) *bioteX*: A suite of Programs for the Collection, Reduction, and Interpretation of Imaging Plate Data, Molecular Structure Corporation, 1995.
(10) *CrystalClear*: Rigaku Corporation, 1999.
(11) *teXsan*: Crystal Structure Analysis Package, Molecular Structure Corporation, 1985 & 1992.
(12) *REQAB4*: Jacobsen, R. A. Private Communication, 1994.
(13) *SIR92*: Altomare, A.; Burla, M. C.; Camalli, M.; Cascarano, M.; Giacovazzo, C.; Guagliardi, A.; Polidoro, G. *J. Appl. Cryst.* **1994**, *27*, 435.
(14) Sheldrick, G. M. *SHELXL-93*: *Program for the Refinement of Crystal Structures*; University of Göttingen: Göttingen, Germany, 1993.

Table 1. NMR Data

compounds	nucleus	δ(multiplicity, intensity, assignment, J(Hz))
2a	$^{11}B^{a,b}$	1.7 (d, B2, J_{BH} 166), −4.2 (d, B10, J_{BH} 144), −5.1 (d, B8, J_{BH} 148), −19.8 (d, B1, J_{BH} 148), −22.9 (d, B9, J_{BH} 157), −24.8 (d, B3, J_{BH} 165), −42.7 (d, B4, J_{BH} 161), −44.1 (dd, B5, J_{BH} 162, J_{PH} 77)
	^{11}B(calcd)^{c}	1.1 (B2), −4.0 (B10), −7.8 (B8), −19.3 (B1), −24.5 (B3), −25.7 (B9), −45.5 (B4), −46.5 (B1)
	$^{11}B-^{11}B^{a,b}$	Observed cross-peaks: B1−B2, −B3, −B4, −B5, −B10; B2−B3, −B5; B3−B4, −B8; B4−B8, −B9, −B10; B5−B10; B8−B9
	$^{1}H\{^{11}B\}^{b,d}$	8.0−7.4 (m, Ph), 4.0 (d, PH, J_{PH} 425) 3.4 (s, BH), 2.8 (s, BH), 2.6 (s, BH), 2.1 (s, 2BH), 1.2 (s, cage CH), 0.7 (s, BH), 0.2 (s, BH), −3.0 (BHB, J_{PH} 26), −3.9 (BHB, J_{PH} 18)
	$^{11}B-^{1}H^{a,b,d}$	Observed cross-peaks: BHB (−3.0 ppm)−B8 (−5.1 ppm), −B9 (−22.9 ppm); BHB (−3.9 ppm) −B10 (−4.2 ppm), −B9 (−22.9 ppm)
	$^{13}C^{b,e}$	(RT) 134.2−123.9 (m, Ph), 6.0 (d, C7, J_{CH} 177); (−83 °C) 134.3−122.0 (m, Ph), 5.2 (dd, C7, J_{CP} 26.7, J_{CH} 168)
	^{13}C(calcd)^{c}	12.1 (C7)
	$^{31}P^{b,f}$	−31.5 (d, P6, J_{PH} 425)
	^{31}P(calcd)^{c}	−23.1 (P6)
2b	$^{11}B^{a,b}$	3.0 (d, B2, J_{BH} 161), −4.8 (d, B8,10, J_{BH} 148), −19.0 (d, B1, J_{BH} 149), −23.0 (d, B9, J_{BH} 149), −25.0 (d, B3, J_{BH} 164), −43.1 (d, B4, J_{BH} 155), −43.9 (dd, B5, J_{BH} 155, J_{BP} 76)
	^{11}B(calcd)^{c}	3.0 (B2), −4.1 (B10), −7.3 (B8), −18.3 (B1), −24.5 (B3), −25.4 (B9), −45.8 (B4), −45.9 (B5)
	$^{11}B-^{11}B^{a,b}$	observed cross-peaks: B1−B2, −B3, −B4, −B5, −B(8,10); B2−B3, −B5; B3−B4, −B(8,10); B5−B(8,10); B(8,10)−B9
	$^{1}H\{^{11}B\}^{b,d}$	4.50 (d, PH, J_{PH} 415), 3.23 (d, PCH_3, J_{PH} 4.5) 2.00 (s, cage CH), −2.00 (BHB, J_{PH} 27), −2.98 (BHB, J_{PH} unresolved)
	$^{11}B-^{1}H^{a,b,d}$	selected observed cross-peaks: BHB (−2.00 ppm)−B8 (−4.8 ppm), −B9 (−23.0 ppm); BHB (−2.98 ppm)−B10 (−4.8 ppm), −B9 (−23.0 ppm)
	$^{13}C^{b,e}$	7.7 (dd, CH_3, J_{CH} 56, J_{CP} 14), 3.5 (d, C7, J_{CH} 174)
	^{13}C(calcd)^{c}	14.8 (CH_3), 7.2 (C7)
	$^{31}P^{b,f}$	−46.8 (d, P6, J_{PH} 415)
	^{31}P(calcd)^{c}	−45.6 (P6)
PSH$^+$2a$^-$	$^{11}B^{a,b}$	−2.8 (d, B8, J_{BH} 146), −6.3 (d, B2, J_{BH} 141), −23.2 (d, B10, J_{BH} br), −32.8 (d, B1, J_{BH} 139), −36.0 (d, B5, J_{BH} 141), −37.4 (d, B4, J_{BH} 141), −39.5 (d, B9, J_{BH} 118), −44.2 (d, B3, J_{BH} 152)
	^{11}B(calcd)^{c}	−1.6 (B2), −3.2 (B8), −23.6 (B10), −31.2 (B1), −37.5 (B4), −40.4 (B5), −42.9 (B9), −44.7 (B3)
	$^{1}H\{^{11}B\}^{b,d}$	7.97−6.91 (m, Ph, PSH^+ and cage Ph−P), 2.73 (s, CH_3, 12, PSH^+), 1.97 (s, cage CH), −2.41 (s, BHB), −4.39 (s, BHB)
	$^{13}C^{b,e}$	147.6−118.2 (m, Ph, PSH^+), 44.4 (d, PSH^+), 10.5 (dd, C7, J_{CP} 43, J_{CH} 160); (−83 °C) 134.3−122.0 (m, Ph), 10.6 (dd, C7, J_{CP} 11, J_{CH} 69)
	^{13}C(calcd)^{c}	17.6 (C6)
	$^{31}P^{b,f}$	−136.4 (s, P6)
	^{31}P(calcd)^{c}	−119.4 (P6)
PSH$^+$2b$^-$	$^{11}B^{a,g}$	−2.0 (d, B8, J_{BH} ∼170), −4.1 (d, B2, br), −22.0 (d, B10, br), −31.4 (d, B1, J_{BH} 170), −33.6 (d, B5, J_{BH} ∼180), −34.9 (d, B4, J_{BH} ∼200), −38.6 (d, B9, J_{BH} ∼110), −44.1 (d, B3, J_{BH} 197)
	^{11}B(calcd)^{c}	2.2 (B8), −3.8 (B2), −28.6 (B10), −28.7 (B1), −31.4 (B5), −31.7 (B4), −42.0 (B9), −48.6 (B3)
PSH$^+$3a$^-$	$^{11}B^{a,h}$	8.4 (d, B5,7, J_{BH} 145), −3.8 (d, B1,4)[i], −4.4 (d, B8,10)[i], −23.2 (d, B3, J_{BH} 150), −30.0 (d, B2, J_{BH} 161)
	^{11}B(calcd)^{c}	12.6 (B5,7), −3.5 (B1,4), −6.1 (B8,10), −19.5 (B3), −27.5 (B2)
	$^{1}H\{^{11}B\}^{d,h}$	8.27−7.55 (m, Ph, PSH^+ and cage Ph−P), 6.54 (s, cage CH), 4.47 (2, BH), 3.50 (2, BH), 3.35 (2, BH), 3.17 (s, CH_3, 12, PSH^+), 1.44 (1, BH), 1.24 (1, BH)
	$^{31}P^{f,h}$	−25.0 (s, P6)
	^{31}P(calcd)^{c}	−41.5 (P6)
PSH$^+$3b$^-$	$^{11}B^{a,b}$	8.9 (d, B5,7, J_{BH} 145), −4.8 (d, B1,4; B8,10), −25.6 (d, B3, J_{BH} 153), −32.1 (d, B2, J_{BH} 153)
	^{11}B(calcd)^{c}	16.6 (B5,7), −3.8 (B1,4), −5.8 (B8,10), −22.0 (B3), −30.9 (B2)
	$^{1}H\{^{11}B\}^{b,j}$	18.7 (PSH^+), 8.04−7.75 (m, Ph, PSH^+), 5.65 (s, cage CH), 3.55 (1, BH), 3.23 (s, CH_3, 12, PSH^+), 2.75, (2, BH), 2.58 (2, BH), 1.56 (P−CH_3), 1.66 (1, BH), 0.74 (1 BH), 0.65 (1 BH), 0.45 (1, BH)
	$^{31}P^{b,k}$	−33.3 (s, P6)
	^{31}P(calcd)^{c}	−67.3 (P6)
PSH$^+$4a$^-$	$^{11}B^{a,g}$	0.3 (d, B2, J_{BH} ∼150), −6.9 (d, B8,10, br), −11.7 (d, B1, J_{BH} 145), −14.8 (d, B3, J_{BH} 148), −19.4 (d, B9, J_{BH} 148), −37.4 (dd, B5, J_{BH} 130, J_{BP} 115), −45.8 (d, B4, J_{BH} 152)
	^{11}B(calcd)^{c}	−1.7 (B2), −8.9 (B10), −9.7 (B8), −12.6 (B1), −17.7 (B3), −24.8 (B9), −39.8 (B5), −49.1 (B4)
	$^{1}H^{d,g}$	18.7 (PSH^+), 7.98−7.31 (m, Ph, PSH^+ and cage Ph−P), 3.16 (s, CH_3, 12, PSH^+), 1.60 (s, cage CH), −1.57 (1, BHB), −2.55 (1, BHB)
	$^{31}P^{g,k}$	−4.2 (q, P6, J_{PB} ∼114)
	^{31}P(calcd)^{c}	−9.5 (P6)
PSH$^+$5a$^-$	$^{11}B^{a,g}$	1.2 (d, B2, J_{BH} 158), −8.7 (d, B10, br), −9.3 (d, B8, J_{BH} br), −14.2 (d, B1, J_{BH} 139), −17.3 (d, B3, J_{BH} ∼130), −18.3 (d, B9, J_{BH} ∼150), −38.1 (dd, B5, J_{BH} 113, J_{BP} 93), −44.4 (d, B4, J_{BH} 142)
	^{11}B(calcd)^{c}	0.3 (B2), −10.2 (B10), −10.5 (B8), −13.6 (B1), −18.1 (B3), −21.0 (B9), −39.8 (B5), −47.2 (B4)
	$^{1}H\{^{11}B\}^{d,g}$	18.7 (PSH^+), 8.16−7.25 (m, Ph, PSH^+ and cage Ph−P), 3.16 (s, CH_3, 12, PSH^+), 2.80 (1, BH), 2.47 (1, BH), 2.26 (1, BH), 2.08 (1, BH), 2.01 (1, BH), 1.93 (1, BH), 1.30 (1, BH), 1.17 (s, cage CH), 0.88 (1, BH), −1.19 (1, BHB), −2.91 (1, BHB)
	$^{31}P^{g,k}$	−9.9 (q, P6, J_{PB} 94)
	^{31}P(calcd)^{c}	10.1 (P6)
PSH$^+$6a$^-$	$^{11}B^{a,b}$	6.0 (d, B2, J_{BH} 138), −7.8 (d, B8, J_{BH} 122), −10.7 (d, B10, J_{BH} 134), −20.5 (d, B1, J_{BH} 139), −24.4 (d, B9, J_{BH} 135), −27.4 (d, B3, J_{BH} 146), −40.7 (dd, B5, J_{BH} >100, J_{BP} 67), −43.6 (d, B4, J_{BH} ∼149), −44.5 (m, B33, J_{BH} ∼164, J_{BP} ∼49)
	^{11}B(calcd)^{c}	5.0 (B2), −10.4 (B8), −12.4 (B10), −21.0 (B1), −28.7 (B9), −28.8 (B3), −43.8 (B33), −46.7 (B4), −47.3 (B5)
	$^{1}H\{^{11}B\}^{b,d}$	19.15 (s, 1, PSH^+), 8.03−7.30 (m, Ph, PSH^+ and cage Ph−P), 3.13 (s, CH_3, 12, PSH^+), 2.95 (1, BH), 2.43 (1, BH), 2.08 (1, BH), 1.86 (1, BH), 1.56 (2, BH), 0.67 (s, cage CH), 0.55 (d, BH_3, J_{HP} 11), 0.47 (1, BH), −0.07 (1, BH), −2.27 (1, BHB), −3.41 (1, BHB)
	$^{31}P^{b,f}$	−65.8 (P6)
	^{31}P(calcd)^{c}	58.6 (P6)
7a	$^{11}B^{a,b}$	−2.4 (d, B10, J_{BH} 147), −4.9 (d, B2, J_{BH} 177), −6.9 (d, B9, J_{BH} 147), −10.0 (d, B1,3,8, J_{BH} ∼150), −29.3 (dd, B5, J_{BH} 147, J_{BP} 89), −42.2 (d, B4, J_{BH} 151)
	^{11}B(calcd)^{c}	−1.9 (B10), −6.9 (B3), −8.1 (B2), −9.0 (B1), −9.9 (B8), −11.1 (B9), −26.0 (B5), −44.1 (B4)
	$^{11}B-^{11}B^{a,b}$	observed cross-peaks: B1−B2; B1−B4; B1−B5; B1−B10; B2−B3; B2−B5; B3−B4; B4−B8; B4−B9; B4−B10; B5−B10
	$^{1}H\{^{11}B\}^{b,d}$	8.31−7.88 (m, Ph), 3.04 (1, BH), 2.96 (s, cage CH), 2.92 (1, BH), 2.77 (2, BH), 2.69 (1, BH), 2.61 (1, BH), 2.12 (1, BH), 1.51 (1, BH), −1.71 (1, BHB), −2.81 (1, BHB)
	$^{13}C\{^{1}H\}^{b,e}$	(RT) 24.5 (s, C7); (−83 °C) 24.5 (dd, C7, J_{CH} 171, J_{CP} 23)
	^{13}C(calcd)^{c}	38.2 (C7)
	$^{31}P^{b,f}$	16.3 (P6)
	^{31}P(calcd)^{c}	58.6 (P6)

[a] 160.5 MHz. [b] CD_2Cl_2. [c] B3LYP/6-311G*//B3LYP-6-311G*. [d] 500.4 MHz. [e] 125.8 MHz. [f] 202.6 MHz. [g] THF-d_8. [h] $CDCl_3$. [i] Coupling not resolved. [j] 200.1 MHz. [k] 145.8 MHz.

Table 2. Crystallographic Data Collection and Structural Refinement Information

	PSH^+3a^-	PSH^+3b^-	PSH^+5a^-
empirical formula	$C_{21}B_8H_{33}N_2P$	$C_{16}B_8H_{31}N_2P$	$C_{25}B_8H_{43}N_2PSO$
formula weight	430.94	368.88	537.12
crystal class	monoclinic	monoclinic	monoclinic
space group	$P2_1/c$ (#14)	$P2_1/n$ (#14)	$P2_1/c$ (#14)
Z	4	4	4
cell constants			
a	10.7136(1) Å	13.9467(2) Å	11.445(2) Å
b	16.1166(2) Å	15.8609(2) Å	10.723(2) Å
c	14.4975(1) Å	10.3485(1) Å	25.458(5) Å
β	90.555(1)°	101.898(1)°	104.249(4)°
V	2503.12(4) Å^3	2239.98(5) Å^3	3028.2(9) Å^3
μ	1.22 cm^{-1}	1.26 cm^{-1}	1.82 cm^{-1}
crystal size, mm	0.35 × 0.20 × 0.18	0.42 × 0.30 × 0.08	0.30 × 0.20 × 0.18
D_{calc}	1.144 g/cm^3	1.094 g/cm^3	1.178 g/cm^3
F(000)	912	784	1144
radiation	Mo−K$_\alpha$ (λ = 0.71069 Å)	Mo−K$_\alpha$ (λ = 0.71069 Å)	Mo−K$_\alpha$ (λ = 0.71069 Å)
2θ range	5.06−50.68 °	5.14−50.7 °	5.04−54.96 °
hkl collected:	$-12 \le h \le 12$; $-19 \le k \le 19$; $-17 \le l \le 17$	$-16 \le h \le 16$; $-19 \le k \le 18$; $-12 \le l \le 12$	$-14 \le h \le 12$; $-11 \le k \le 13$; $-32 \le l \le 33$
no. reflections measured	19744	16686	19957
no. unique reflections	4547 (R_{int} = 0.0272)	3968 (R_{int} = 0.0426)	6720 (R_{int} = 0.0441)
no. observed reflections	4203 ($F > 4\sigma$)	3634 ($F > 4\sigma$)	5293 ($F > 4\sigma$)
no. reflections used in refinement	4547	3968	6720
no. parameters	421	280	483
R indices ($F > 4\sigma$)[a]	R_1 = 0.0503	R_1 = 0.0710	R_1 = 0.0728
	wR_2 = 0.1120	wR_2 = 0.1391	wR_2 = 0.1339
R indices (all data)	R_1 = 0.0560	R_1 = 0.0804	R_1 = 0.1009
	wR_2 = 0.1150	wR_2 = 0.1433	wR_2 = 0.1449
GOF	1.145	1.272	1.119
final difference peaks, e/Å^3	+0.213, −0.247	+0.202, −0.322	+0.659, −0.434

[a] $R_1 = \sum||F_o| - |F_c||/\sum|F_o|$; $wR_2 = \{\sum w(F_o^2 - F_c^2)^2/\sum w(F_o^2)^2\}^{1/2}$.

Computational Studies. The DFT/GIAO/NMR method,[15] using the Gaussian 94 program,[16] was used in a manner similar to that previously described.[1,8,17] The geometries were fully optimized at the B3LYP/6-311G* level within the specified symmetry constraints (using the standard basis sets included) on a (4)-processor Origin 2000 computer running IRIX 6.5.5 or a (6)-processor Power Challenge XL computer running IRIX 6.5.6. A vibrational frequency analysis was carried out on each optimized geometry at the B3LYP/6-311G* level with a true minimum found for each structure (i.e., possessing no imaginary frequencies). The NMR chemical shifts were calculated at the B3LYP/6-311G* level using the GIAO option within Gaussian 94. ^{11}B NMR GIAO chemical shifts are referenced to $BF_3{\cdot}O(C_2H_5)_2$ using an absolute shielding constant of 102.24.[18,19] The ^{13}C NMR GIAO chemical shifts were referenced to TMS using an absolute shielding constant of 184.38 and were corrected according to the method described by Schleyer.[20] The ^{31}P NMR GIAO chemical shifts were first referenced to PH_3 using an absolute shielding constant of 557.2396 ppm and then converted to the H_3PO_4 reference scale using the experimental value of $\delta(PH_3) = -240$ ppm.[21]

(15) Yang, X.; Jiao, H.; Schleyer, P. v. R. *Inorg. Chem*. **1997**, *36*, 4897−4899 and references therein.
(16) Frisch, M. J.; Trucks, G. W.; Schlegel, H. B.; Gill, P. M. W.; Johnson, B. G.; Robb, M. A.; Cheeseman, J. R.; Keith, T.; Peterson, G. A.; Montgomery, J. A.; Raghavachari, K.; Al-Laham, M. A.; Zakrzewski, V. G.; Ortiz, J. V.; Foresman, J. B.; Cioslowski, J.; Stefanov, B. B.; Nanayakkara, A.; Challacombe, M.; Peng, C. Y.; Ayala, P. T.; Chen, W.; Wong, M. W.; Andres, J. L.; Replogle, E. S.; Gomperts, R.; Martin, R. L.; Fox, D. J.; Binkley, J. S.; Defrees, D. J.; Baker, J.; Stewart, J. P.; Head-Gordon, M.; Gonzalez, C.; Pople, J. A. *Gaussian 94*, revision E.2; Gaussian, Inc.: Pittsburgh, PA, 1995.
(17) (a) Kadlecek, D. E.; Carroll, P. J.; Sneddon, L. G. *J. Am. Chem. Soc.* **2000**, *122*, 10868−10877. (b) Shedlow, A. M.; Sneddon, L. G. *Collect. Czech. Chem. Commun.* **1999**, *64*, 865−882. (c) Bausch, J. W.; Rizzo, R. C.; Sneddon, L. G.; Wille, A. E.; Williams, R. E. *Inorg. Chem.* **1996**, *35*, 131−135.
(18) Tebben, A. J. Master's Thesis, Villanova University, 1997.
(19) Tebben, A. J.; Bausch, J. W. private communication.
(20) Maerker, C.; Schleyer, P. v. R.; Salahub, D. R.; Malkina, O. L.; Malkin, V. G. private communication.
(21) Crutchfield, M. M.; Dungan, C. H.; Letcher, L. H.; Mark, V.; Van Wazer, J. R. *Top. Phosphorus Chem.* **1967**, *5*, 1−487.

Results and Discussion

As shown in eq 1, reaction of *arachno*-4-CB_8H_{14} (**1**) with an excess of Proton Sponge and an equivalent of $RPCl_2$ (R = C_6H_5 (**a**), CH_3 (**b**)) yielded a mixture of the new 10-vertex phosphamonocarbaboranes *exo*-6-R-*arachno*-6,7-PCB_8H_{12} (**2a** and **2b**) and PSH^+6-R-*nido*-6,9-$PCB_8H_9^-$ (**PSH^+3a$^-$** and **PSH^+3b$^-$**).

$$\underset{\mathbf{1}\ \mathrm{R} = \mathrm{C_6H_5}\ (\mathbf{a}),\ \mathrm{CH_3}\ (\mathbf{b})}{\textit{arachno}\text{-}4\text{-}CB_8H_{14}} + RPCl_2 \xrightarrow[-2\ PSH^+Cl^-]{+\text{exs PS}}$$

$$1 - x\ \textit{exo}\text{-}6\text{-}R\text{-}\textit{arachno}\text{-}6,7\text{-}PCB_8H_{12} + \underset{\mathbf{2a},\ \mathbf{2b}}{}$$

$$x PSH^+6\text{-}R\text{-}\textit{nido}\text{-}6,9\text{-}PCB_8H_9^- + xH_2 \quad (1)$$
$$\mathbf{PSH^+3a^-},\ \mathbf{PSH^+3b^-}$$

The reactions with $C_6H_5PCl_2$ gave relative yields of **2a** and **PSH^+3a$^-$** that were largely independent of reaction conditions, with the major product **2a** being obtained in greater than 95% isolated yield. However, the relative amounts of **2b** and **PSH^+3b$^-$** that were obtained from the reactions with CH_3PCl_2 varied according to the reaction temperature and initial concentration of **1**. As described in the Experimental Section, room-temperature reactions with lower concentrations of **1** (2.0 mmol of **1** in 40 mL of THF) gave high yields (>90%) of **2b** and only small amounts of **PSH^+3b$^-$**, while reactions performed at 0 °C with a higher concentration of **1** (2.0 mmol of **1** in 20 mL of THF) afforded up to 92% **PSH^+3b$^-$**. Separation of the products could easily be accomplished because of their differences in solubility. Thus, the neutral products **2a** and **2b** were soluble in toluene, while the ionic products **PSH^+3a$^-$** and **PSH^+3b$^-$** were insoluble. **PSH^+3a$^-$** and **PSH^+3b$^-$** were also soluble in THF and could thus be easily separated from the insoluble reaction byproduct, PSH^+Cl^-.

While the above in situ dehydrohalogenation sequence yielded a mixture of both the **2** and $\mathbf{3}^-$ products, it was found that reactions of $RPCl_2$ employing the *arachno*-4-$CB_8H_{12}^{2-}$ ($\mathbf{1}^{2-}$) dianion[8] gave only the *exo*-6-R-*arachno*-6,7-PCB_8H_{12} products in 94% (**2a**) and 80% (**2b**) isolated yields.

$$\underset{\mathbf{Na_2 1^{2-}}}{Na_2[\textit{arachno}\text{-}4\text{-}CB_8H_{12}^{2-}]} + RPCl_2 \rightarrow \underset{\mathbf{2a},\ \mathbf{2b}}{\textit{exo}\text{-}6\text{-}R\text{-}\textit{arachno}\text{-}6,7\text{-}PCB_8H_{12}} + 2\ NaCl \quad (2)$$

The ^{11}B NMR spectra of $\mathbf{PSH^+3a^-}$ and $\mathbf{PSH^+3b^-}$ are consistent with C_S symmetry, each showing five doublets of intensities 2:2:2:1:1. Likewise, their boron-decoupled ^1H NMR spectra show, in addition to the PSH^+ and the Me or Ph resonances, five singlets corresponding to the terminal BH protons and one singlet attributed to the cage CH proton.

Given their 24 skeletal electron counts ($n + 2$ skeletal electron pairs), the structures of the $\mathbf{3a}^-$ and $\mathbf{3b}^-$ anions would be expected to be similar to those found for other 10-vertex, nido-clusters, such as the thiamonocarbaborane *nido*-6,9-$SCB_8H_9^-$ [22] and tricarbadecaborane 6-CH_3-*nido*-5,6,9-$C_3B_7H_9^-$ [23] monoanions, with a cage structure based on an octadecahedron missing its six-coordinate vertex. Single-crystal, X-ray structural determinations of PSH^+6-(C_6H_5)-*nido*-6,9-$PCB_8H_9^-$ ($\mathbf{PSH^+3a^-}$) and PSH^+6-CH_3-*nido*-6,9-$PCB_8H_9^-$ ($\mathbf{PSH^+3b^-}$), in fact, confirmed this geometry. Since there were no significant differences in the structures of the two anions, only the structure of $\mathbf{3a}^-$ is shown in Figure 1, where it can be seen that the anion has a puckered six-membered open face with the phosphorus and carbon atoms adopting the three-coordinate 6 and 9 positions that are above the plane of the other four borons (B5, B7, B8, B10) on the face. Such low-coordinate sites are known to be favored by more electron-rich elements,[17c,24] and the sulfur and carbon atoms occupy the same positions in the known isoelectronic *nido*-6,9-$SCB_8H_9^-$ anion.[22] Selected intracage distances and angles are given in the Figure 1 caption and are all in the normal ranges.

DFT calculations at the B3LYP/6-311G* level on the structures of $\mathbf{3a}^-$ and $\mathbf{3b}^-$ yielded optimized geometries $\mathbf{IIIa}^-$ and $\mathbf{IIIb}^-$ that are in excellent agreement with the crystallographically determined structures, as can be seen in Figure 1 where the optimized geometry $\mathbf{IIIa}^-$ is compared to that of the crystallographically determined structure of $\mathbf{3a}^-$. Likewise, the GIAO calculated chemical shifts and resonance assignments given in Table 1 are in accord with the experimental values obtained from the 1 and 2D NMR studies.

Given the similarity of the structures of $\mathbf{3a}^-$ and $\mathbf{3b}^-$ to that of *nido*-6,9-$SCB_8H_9^-$, it might be expected that the structure for the arachno-compounds **2a** and **2b** should likewise be similar to that found for their isoelectronic thiamonocarbaborane analogue, *arachno*-6,9-SCB_8H_{12}.[22] However, as illustrated by the ^{11}B NMR spectra of **2a** presented in Figure 2, the ^{11}B NMR

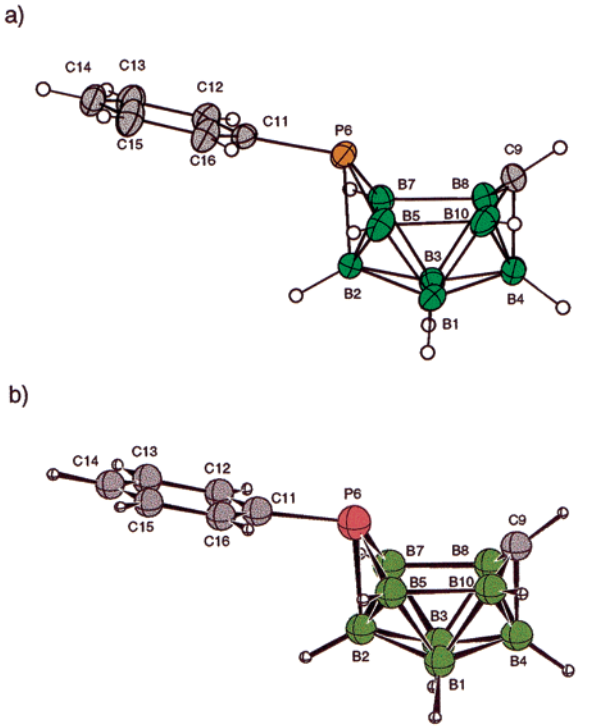

Figure 1. Comparison of the crystallographically determined structure of the 6-C_6H_5 -*nido*-6,9-$PCB_8H_9^-$ anion in $\mathbf{PSH^+3a^-}$ (a) with that of the DFT calculated geometry $\mathbf{IIIa}^-$ (b). Selected bond distances (Å) and angles (°) in $\mathbf{PSH^+3a^-}$: P6−B7, 1.891(2); B7−B8, 1.861(3); B8−C9, 1.529(4); B10−C9, 1.523(4); B5−B10, 1.871(4); B5−P6, 1.897(3); C9−B4, 1.681(3); P6−B2, 2.016(2); P6−C11, 1.821(2); C11−P6−B2, 104.07(9); C11−P6−B5, 116.8(1); C11−P6−B7, 116.3(1); B7−P6−B5, 98.5(1); B10−C9−B8, 119.1(2). Selected calculated bond distances (Å) and angles (°) in $\mathbf{IIIa}^-$: P6−B7, 1.938; B7−B8, 1.868; B8−C9, 1.536; B10−C9, 1.536; B5−B10, 1.868; B5−P6, 1.938; C9−B4, 1.708; P6−B2, 2.046; P6−C11, 1.850; C11−P6−B2, 100.2; C11−P6−B5, 114.4; C11−P6−B7, 114.5; B7−P6−B5, 96.7; B10−C9−B8, 120.0.

spectra of **2a** and **2b** each showed eight separate resonances, indicating that they have C_1 symmetry rather than the C_S symmetry that has been confirmed for *arachno*-6,9-SCB_8H_{12}.[22] The ^1H NMR spectra of **2a** (Figure 3) and **2b** also indicate C_1 symmetry, showing eight terminal BH and two different bridge hydrogen resonances. Furthermore, while the ^1H NMR spectrum of *arachno*-6,9-SCB_8H_{12} contains a CH_2 resonance, the spectra of **2a** and **2b** exhibit only a single CH resonance. The most unique feature of the ^1H NMR spectra of **2a** and **2b** is that they both contain a PH resonance (**2a**, $J_{PH} = 425$; **2b**, $J_{PH} = 415$ Hz). The presence of a PH group is also supported by the ^{31}P NMR spectra which show a doublet at −31.7 ppm for **2a** ($J_{PH} = 425$) and at −45.6 ppm for **2b** ($J_{PH} = 415$ Hz). The observed PH coupling constants are consistent with previously reported values for clusters containing a P(R)H moiety. For example, the bridging phosphaborane cluster, $[B_5H_7P(H)(CH(OSiMe_3)(^tBu))]^{1-}$ has a $J_{PH} = 421$ Hz, while the neutral clusters, $B_5H_7P(H)(CH(OSiMe_3)(^tBu))$ and $B_5H_8P(H)(CH(OSiMe_3)$(adamantyl) display coupling constants of $J_{PH} = 410$ and $J_{PH} = 406$ Hz, respectively.[25]

The 125.7 MHz ^{13}C NMR spectra of **2a** (Figure 4) and **2b** support the ^1H NMR data, each showing a broad doublet cage CH resonance (Figure 4b) at room temperature and not the CH_2

(22) (a) Holub, J.; Kennedy, J. D.; Jelínek, T.; Stíbr, B. *J. Chem. Soc., Dalton Trans.* **1994**, 1317−1323. (b) Holub, J.; Jelínek, T.; Plesek, J.; Stíbr, B.; Hermanek, S.; Kennedy, J. D. *J. Chem. Soc., Chem. Commun.* **1991**, 1389−1390.
(23) (a) Kang, S. O.; Furst, G. T.; Sneddon, L. G. *Inorg. Chem.* **1989**, *28*, 2339−2347. (b) Wasczcak, M. D.; Wang, Y.; Garg, A.; Geiger, W. E.; Kang, S. O.; Carroll, P. J.; Sneddon, L. G. *J. Am. Chem. Soc.* **2001**, *123*, 2783−2790.
(24) Williams, R. E. *Adv. Inorg. Chem. Radiochem.* **1976**, *18*, 67−142.
(25) Miller, R. W.; Donaghy, K. J.; Spencer, J. T. *Organometallics* **1991**, *10*, 1161−1172.

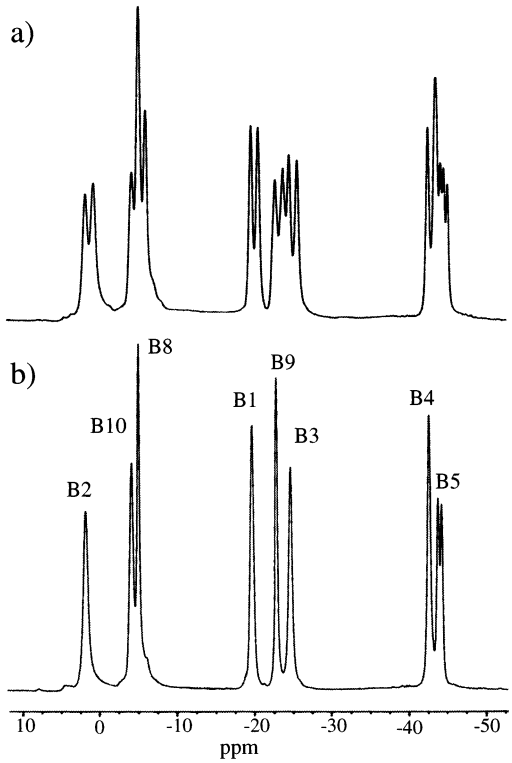

Figure 2. 160.5 MHz ^{11}B NMR spectra of **2a**: (a) proton-coupled, (b) proton-decoupled.

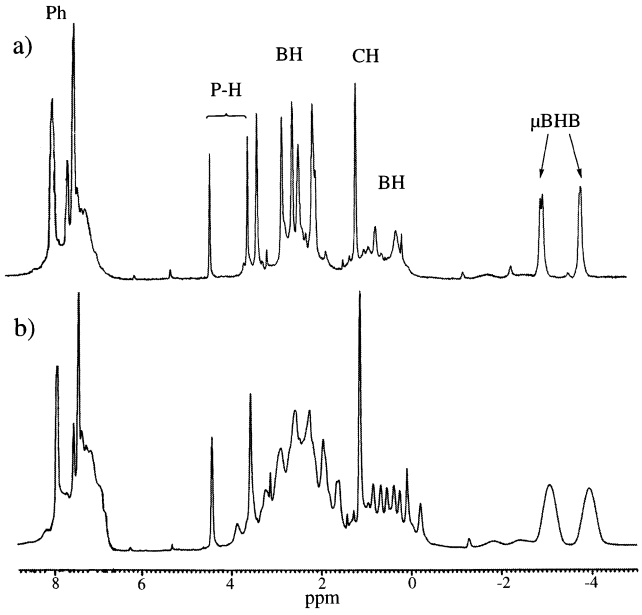

Figure 3. 500.4 MHz ^{1}H NMR spectra of **2a**: (a) boron-decoupled, (b) boron-coupled.

resonance found for *arachno*-6,9-SCB_8H_{12}. At −83 °C, the doublet resonance sharpens (Figure 4d) because of quenching of carbon−boron scalar coupling[26] and shows additional fine phosphorus coupling (J_{CP} = 26.7 Hz) which strongly supports a cage framework in which the phosphorus and carbon occupy adjacent positions.

Unfortunately, both **2a** and **2b** are oily solids, thus crystallographic determinations of their structures were not possible. Therefore, DFT/GIAO computational studies were undertaken to confirm their structures. For compound **2b**, numerous

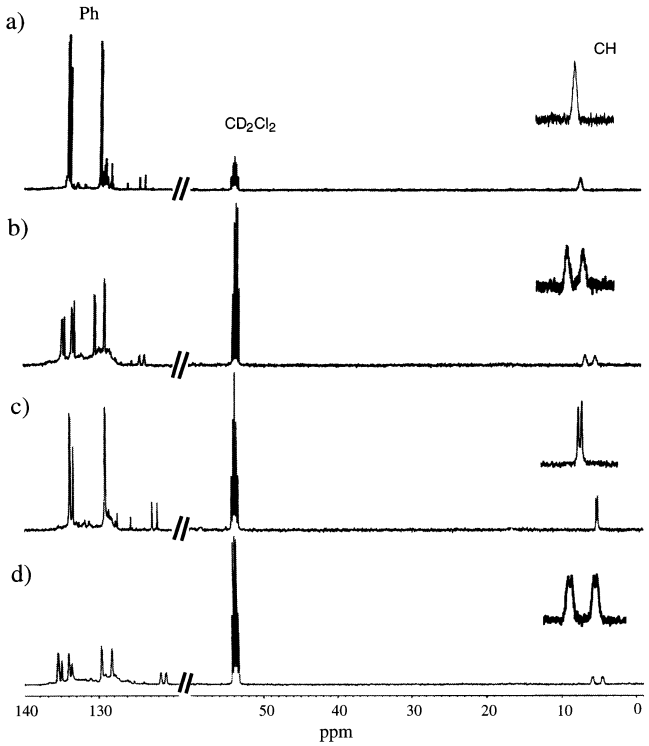

Figure 4. 125.8 MHz ^{13}C NMR spectra of **2a**: (a) proton-decoupled spectrum at room temperature; (b) proton coupled spectrum at room temperature; (c) proton-decoupled spectrum at −83 °C; (d) proton-coupled spectrum at −83 °C.

isomeric structures were investigated, some of which are shown in Figure 5. The C_S symmetry structure **IIb1** in which the phosphorus and carbon atoms, like in the *arachno*-6,9-SCB_8H_{12} cluster, are situated in the low-coordinate 6, 9 positions proved to be of lowest energy. However, both the symmetry and GIAO calculated chemical shifts for this isomer are inconsistent with those observed for **2a** and **2b**. Among the C_1 symmetry isomers, the **IIb2** structure with the carbon in one of the three-coordinate vertexes (9-position), but with the phosphorus in the higher coordinate 7-position, was next lowest in energy, being only 2.1 kcal/mol higher than the C_S structure. Higher still in energy were the exo and endo structures **IIb3** and **IIb4** with the phosphorus in the favored three-coordinate 6-vertex, but with the carbon in the higher coordinate 7-vertex adjacent to the phosphorus. In the highest energy isomer **IIb5**, the carbon and phosphorus are in the nonadjacent 6 and 8 positions but have the same coordination numbers as in **IIb3** and **IIb4**. Given the tendency of electron-rich elements to separate, it is perhaps surprising that isomer **IIb5** proved to be of higher energy than **IIb3** and **IIb4**.

Examination of the GIAO calculated ^{11}B, ^{31}P, and ^{13}C NMR shifts and ^{11}B assignments for each of the above isomers demonstrated that only structure **IIb3** (and that of the calculated structure, **IIa3**, for the phenyl analog) is in complete agreement with the observed NMR data for **2b** (and **2a**). As shown in Figure 6a for **IIa3**, in this isomer the phosphorus and carbon atoms are on the six-membered open face of the cluster with the phosphorus atom situated in one of the three-coordinate

(26) (a) Wrackmeyer, B. In *Progress in NMR Spectroscopy;* Emsley, J. W., Feeney, J., Sutcliffe, L. H., Eds.; Pergamon: New York, 1979; Vol. 12, pp 227−259. (b) Gragg, B. R.; Layton, W. J.; Niedenzu, K. *J. Organomet. Chem.* **1977**, *132*, 29−36.

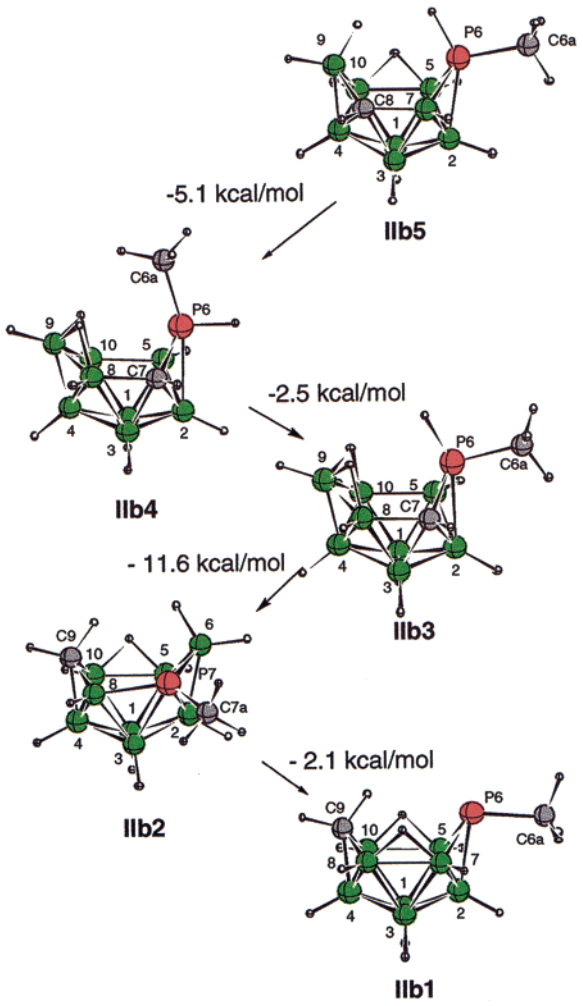

Figure 5. Energy comparisons for DFT optimized isomeric structures of **2b**.

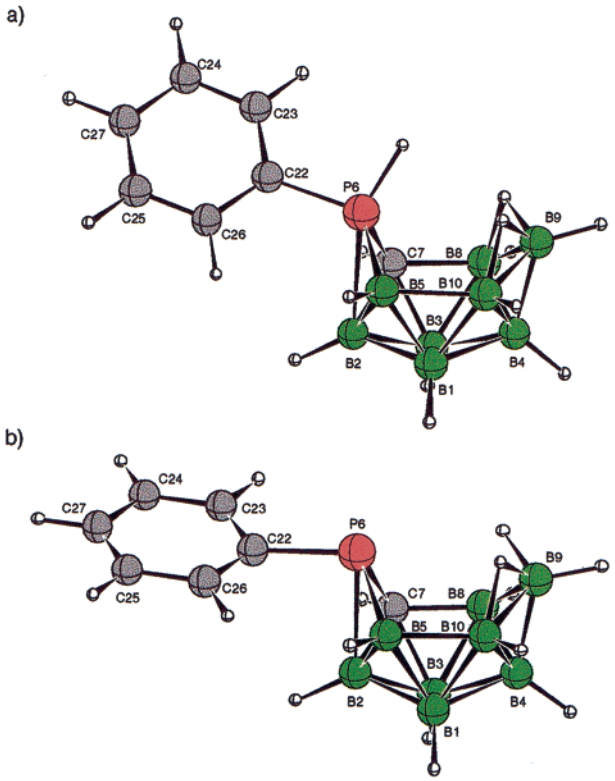

Figure 6. Optimized geometries and selected calculated bond distances (Å) and angles (°) for structures: (a) **IIa3**, P6−H, 1.435; P6−B2, 2.232; P6−B5, 1.884; P6−C7, 1.819, C7−B8, 1.677; B8−B9, 1.815; B9−B10, 1.825; B5−B10, 1.845; P6−C22, 1.817; C22−P6−B2, 105.3; C22−P6−B5, 119.6; C22−P6−C7, 113.3; C7−B6−B5, 93.9; B10−B9−B8, 101.1; P6H−P6−C22, 100.7; P6H−P6−C7, 107.0; P6H−P6−B5, 122.2. (b) **IIa**$^-$**2**, P6−B2, 2.204; P6−B5, 1.984; P6−C7, 1.925, C7−B8, 1.606; B8−B9, 1.852; B9−B10, 1.877; B5−B10, 1.770; P6−C22, 1.881; C22−P6−B2, 90.0; C22−P6−C7, 106.2; C22−P6−B5, 109.2; C7−B6−B5, 89.7; B10−B9−B8, 99.8.

vertexes (6-position), while the carbon atom occupies the adjacent higher energy four-coordinate 7-vertex. Bridge protons span the B8−B9 and B9−B10 edges. The NMR data for **2a** and **2b** and structures **IIa3** and **IIb3** are compared in Table 1, where it can be seen that there is excellent agreement between the observed and calculated NMR chemical shifts and assignments. The phosphorus fine-coupling found for the resonance near −44 ppm in the ^{11}B NMR spectra of compounds **2a** (J_{PB} ∼ 77 Hz) and **2b** (J_{PB} ∼ 76 Hz) is likewise in agreement with the GIAO assignment of this resonance to the B5 boron adjacent to P6. The fact that the in situ dehydrohalogenation reactions yield compounds **2a** and **2b** having the adjacent phosphorus-carbon cage structure **IIb3** instead of the energically favored **IIb1** structure, is undoubtedly a result of the mild reaction conditions which allow the isolation of kinetic rather than thermodynamic products.

Final confirmation of the cage framework was obtained, as reported in the following paper,[4] by the crystallographic characterizations of two transition-metal derivatives of **2a**, *endo*-6-[(η^5-C_5H_5)Fe(CO)$_2$]-*exo*-6-Ph-*arachno*-6,7-PCB_8H_{11} and *exo*-6-[(Mn(CO)$_5$]-*endo*-6-Ph-*arachno*-6,7-PCB_8H_{11} complexes. In both complexes, the phosphacarbaborane ligand has, as proposed in **2a** and **2b**, a six-membered puckered open face containing two bridge hydrogens and a 6-position PR group adjacent to the cage CH in the 7-position. The two structures differ in their alternate exo and endo positioning of the metal and R substituents at the phosphorus, thus illustrating that both conformations are possible. For **2a** and **2b**, the DFT/GIAO calculations in conjunction with the NMR data indicate that the Me and Ph groups are substituted at the exo position of the phosphorus with the hydrogen in the endo position. However, as discussed in the following paper,[4] the *endo*-Me isomer **IIb4** proved to be only 2.5 kcal/mol less stable than the *exo*-isomer **IIb3**.

The formation of *exo*-6-R-*arachno*-6,7-PCB_8H_{12} (**2a** and **2b**) via the *arachno*-4-$CB_8H_{12}^{2-}$ (**1**$^{2-}$) dianion probably follows a pathway similar to that given in Figure 7. The *arachno*-4-$CB_8H_{12}^{2-}$ anion has been shown to have the structure shown in the figure, resulting from deprotonation of one bridging and the *endo*-CH hydrogen from the parent *arachno*-4-CB_8H_{14}.[8] Reaction of this dianion with $RPCl_2$ in the manner shown in the figure with insertion of the phosphorus between the vacant B5−B6 edge and *endo*-carbon position (structure **A**), accompanied by proton transfer to the basic phosphorus endo position then leads in a straightforward manner to the structures observed for **2a** and **2b**.

The formation of the *exo*-6-R-*arachno*-6,7-PCB_8H_{12} (**2**) and PSH^+6-R-*nido*-6,9-$PCB_8H_9^-$ (**3**$^-$) products from the reactions of the *arachno*-4-$CB_8H_{13}^-$ (**1**$^-$) monoanion with $RPCl_2$ in the presence of Proton Sponge are more complex. Attempts to thermally induce molecular hydrogen loss from either **2** or **2**$^-$ to form **3**$^-$ were unsuccessful, thus indicating that the formation

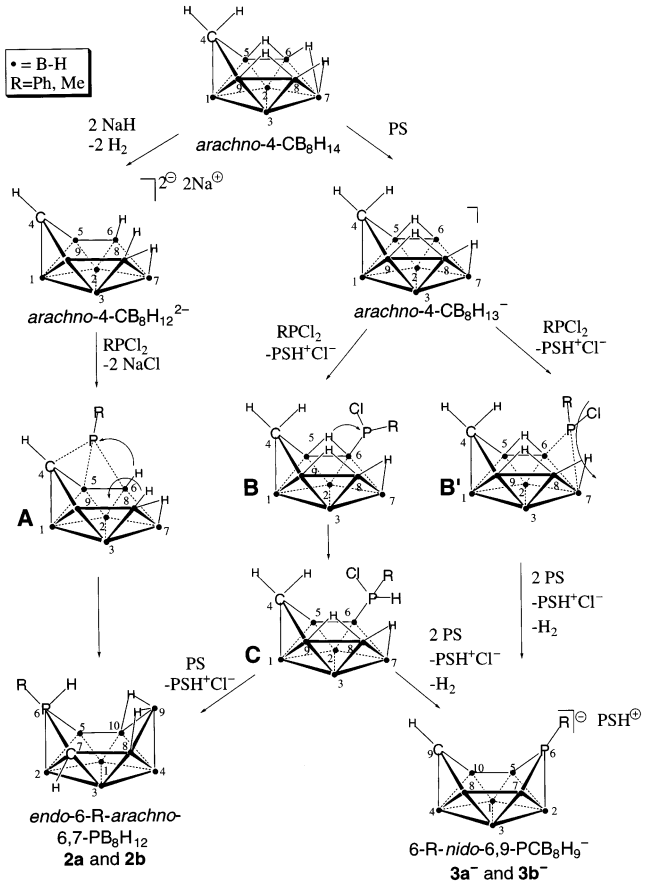

Figure 7. Possible reaction steps leading to the formation of **2** and **3**$^-$.

of **3**$^-$ does not follow from **2** or **2**$^-$. The formation of the **2** and **3**$^-$ products are most likely a consequence of competing substitution/dehydrohalogenation steps, such as those depicted in Figure 7. The **1**$^-$ monoanion is initially generated by deprotonation of the B6−B7 bridge hydrogen of **1** by Proton Sponge.[6] The reaction of **1**$^-$ with $RPCl_2$ could then result in substitution of the RClP− group at either the terminal B6 (structure **B**) or the B6−B7 bridging (structure **B′**) cage-position. A Proton Sponge initiated dehydrohalogenation of **B′**, involving the bridging hydrogen at the B7−B8 edge, accompanied by both loss of molecular hydrogen and deprotonation then leads to the structure observed for the **3**$^-$ anions. On the other hand, if **B** is formed instead of **B′**, then proton transfer from a bridge to the terminal RClP− group could occur as indicated to generate the base adduct, *exo*-6-(RPHCl)-*arachno*-4-CB_8H_{12} (structure **C**), with **C** being another example of the known series of *exo*-6-L-*arachno*-4-CB_8H_{12} compounds.[27] Such a migration of a cluster proton to an exopolyhedral Ph_2P group has previously been observed by Zakharkin et al.[28] during the reaction between diphenylchlorophosphine and *nido*-7,8-$C_2B_9H_{12}^-$ to yield 9-Ph_2-PH-*nido*-7,8-$C_2B_9H_{11}$. A Proton Sponge initiated dehydrohalogenation from **C** involving the acidic *endo*-CH hydrogen would then result in the formation of **2** where the phosphorus and carbon atoms are in adjacent positions, while a dehydrohalogenation involving the B7−B8 bridging proton accompanied by loss of molecular hydrogen and deprotonation would instead generate **3**$^-$. At this point, it is not clear why the reactions with $C_6H_5PCl_2$ yield almost exclusively **2b**, while the reactions with CH_3PCl_2 give, depending upon reaction conditions, high yields of either **2a** or **3a**$^-$. However, it may be that the more electron-donating CH_3P unit helps facilitate the loss of molecular hydrogen that is a key step (from either **B′** or **C**) that is needed to form the **3**$^-$ structure.

Attempts to form the neutral compound, 6-R-*nido*-6,9-PCB_8H_{10}, by protonation of **3**$^-$ with strong acids such as concentrated H_2SO_4 gave no reaction. However, as shown in eq 3, **2a** and **2b** underwent reversible deprotonation/protonation reactions. Thus, deprotonation of **2a** and **2b** by NaH, BuLi, or Proton Sponge resulted in the formation of the **2a**$^-$ and **2b**$^-$ monoanions. Reprotonation of the Na^+ or Li^+ salts with HCl·OEt_2, or the Proton Sponge salt with concentrated H_2SO_4, resulted in the regeneration of the neutral *exo*-6-R-*arachno*-6,7-PCB_8H_{12} compounds.

$$\underset{\mathbf{2a},\ \mathbf{2b}}{\textit{exo}\text{-6-R-}\textit{arachno}\text{-6,7-}PCB_8H_{12}} \overset{-H^+}{\underset{+H^+}{\rightleftharpoons}} \underset{\mathbf{2a}^-,\ \mathbf{2b}^-}{\textit{exo}\text{-6-R-}\textit{arachno}\text{-6,7-}PCB_8H_{11}^-} \quad (3)$$

As discussed below, the **2**$^-$ monoanions are very air sensitive and it was not possible to isolate them in pure form; however, their structures can be confidently assigned on the basis of the spectroscopic and computational studies. The ^{11}B NMR spectra of the **2**$^-$ monoanions each showed eight separate doublet resonances indicative of C_1 symmetry. The 125.7 MHz ^{13}C NMR spectra of **2a**$^-$ contained a CH resonance and the ^1H NMR spectra of both anions showed, in addition to the Me or Ph resonances, two different bridge hydrogen resonances and a CH resonance but no PH resonance. Deprotonation at the phosphorus atom was further confirmed by their ^{31}P NMR spectra, which showed a singlet resonance for both **2a**$^-$ and **2b**$^-$ rather than doublet resonances found in the spectra of **2a** and **2b**.

DFT/GIAO calculations of the possible structures of the **2a**$^-$ and **2b**$^-$ anions yielded optimized geometries **IIa**$^-$**2** and **IIb**$^-$**2** with calculated ^{11}B NMR shifts and assignments in good agreement with the experimental values. As shown in Figure 6b for structure **IIa**$^-$**2**, these structures result from deprotonation at phosphorus, with the phosphorus and carbon remaining adjacent and the phenyl (and methyl) still in the phosphorus exo position. As depicted in Figure 8, structure **IIb**$^-$**2** was, in fact, the lowest energy C_1 symmetry methyl isomer in which the carbon and phosphorus remained in adjacent positions but is 3.1 kcal/mol less stable than the C_S symmetry isomer **IIb**$^-$**1** in which both the phosphorus and carbon occupy the favored low-coordinate 6 and 9 positions.

Upon exposure to air, the **2a**$^-$ anion readily reacted to form the oxygen adduct **4a**$^-$.

$$\underset{\mathbf{PSH^+2a^-}}{PSH^+\text{6-}(C_6H_5)\text{-}\textit{arachno}\text{-6,7-}PCB_8H_{11}^-} + 1/2\ O_2 \rightarrow \underset{\mathbf{PSH^+4a^-}}{PSH^+\textit{endo}\text{-6-O-}\textit{exo}\text{-6-}(C_6H_5)\text{-}\textit{arachno}\text{-6,7-}PCB_8H_{11}^-} \quad (4)$$

As shown in eq 5 and 6, the corresponding anionic sulfur (**PSH**$^+$**5a**$^-$) and borane adducts (**PSH**$^+$**6a**$^-$) were also formed

(27) Plesek, J.; Stíbr, B.; Fontaine, X. L. R.; Jelínek, T.; Thornton-Pett, M.; Hermanek, S.; Kennedy, J. D. *Inorg. Chem.* **1994**, *33*, 2994−3002.
(28) Zakharkin, L. I.; Ol'shevskaya, V. A.; Zhigareva, G. G.; Antonovich, V. A.; Petrovskii, P. V.; Yanovskii, A. I.; Polyakov, A. V.; Struchkov, Y. T. *Metalloorg. Khim.* **1989**, *2*, 1274−1282.

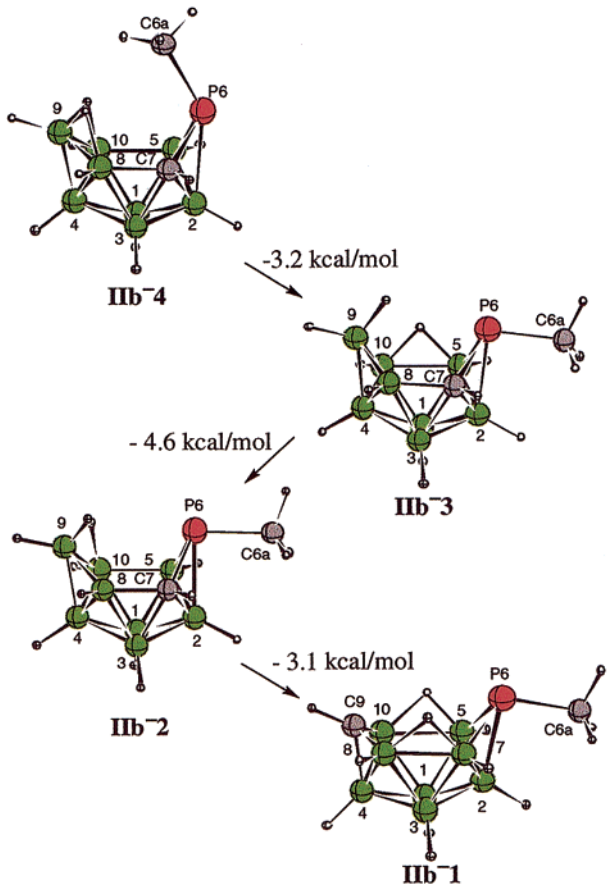

Figure 8. Energy comparisons for DFT optimized isomeric structures of **2b**$^-$.

by the reaction of **PSH**$^+$**2a**$^-$ with elemental sulfur and BH_3·THF, respectively.

$$PSH^+6\text{-}(C_6H_5)\text{-}arachno\text{-}6,7\text{-}PCB_8H_{11}^- + 1/8\ S_8 \rightarrow \underset{\mathbf{PSH^+2a^-}}{}$$
$$PSH^+endo\text{-}6\text{-}S\text{-}exo\text{-}6\text{-}(C_6H_5)\text{-}arachno\text{-}6,7\text{-}PCB_8H_{11}^- \quad (5)$$
$$\mathbf{PSH^+5a^-}$$

$$PSH^+6\text{-}(C_6H_5)\text{-}arachno\text{-}6,7\text{-}PCB_8H_{11}^- + BH_3{\cdot}THF \rightarrow \underset{\mathbf{PSH^+2a^-}}{}$$
$$PSH^+endo\text{-}6\text{-}BH_3\text{-}exo\text{-}6\text{-}(C_6H_5)\text{-}arachno\text{-}6,7\text{-}PCB_8H_{11}^-$$
$$\mathbf{PSH^+6a^-} \quad (6)$$

Reaction of **PSH**$^+$**2a**$^-$ with bromine resulted in heterolytic cleavage of the Br−Br bond with a formal bromonium ion transfer to the cage phosphorus to generate the neutral Br-substituted derivative *endo*-6-Br-*exo*-6-(C_6H_5)-*arachno*-6,7-PCB_8H_{11} (**7a**) as given in eq 7.

$$PSH^+6\text{-}(C_6H_5)\text{-}arachno\text{-}6,7\text{-}PCB_8H_{11}^- + Br_2 \rightarrow \underset{\mathbf{PSH^+2a^-}}{}$$
$$endo\text{-}6\text{-}Br\text{-}exo\text{-}6\text{-}(C_6H_5)\text{-}arachno\text{-}6,7\text{-}PCB_8H_{11}^- + PSH^+Br^- \quad (7)$$
$$\mathbf{7a}$$

The NMR spectra of **4a**$^-$, **5a**$^-$, **6a**$^-$, and **7a** have many common features strongly supporting similar cage frameworks

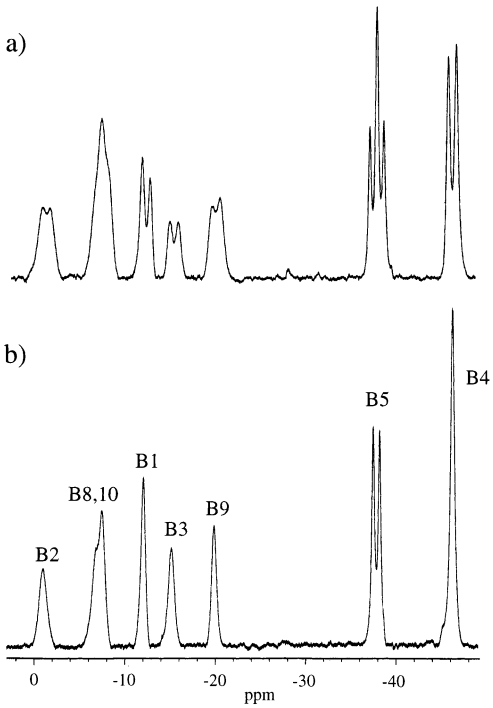

Figure 9. 160.5 MHz ^{11}B NMR spectra of **4a**$^-$: (a) proton-coupled, (b) proton-decoupled.

for these compounds. Thus, the single resonance observed in the ^{31}P NMR spectrum of each compound showed no J_{PH} coupling indicating that substitution at the phosphorus had occurred. Their boron-decoupled ^{1}H NMR spectra each showed, in addition to the appropriate phenyl or methyl signals, resonances attributable to eight terminal BH protons, a cage-CH proton, and two inequivalent bridging protons. The spectrum of **6a**$^-$ also contained a doublet at 0.54 ppm with $J_{HP} = 11$ Hz that can be assigned to the protons of the phosphorus-bonded borane group. The ^{11}B NMR spectra of the compounds again indicate C_1 symmetry and, as illustrated in the spectra of **4a**$^-$ shown in Figure 9, **4a**$^-$, **5a**$^-$, and **7a** each have a resonance at high field (−37.4, −38.1, and −29.3 ppm, respectively) showing J_{BP} fine-coupling characteristic of a boron (B5) adjacent to a phosphorus. For **6a**$^-$, two of the nine resonances, −40.7 ppm ($J_{BP} = 67$ Hz) and −44.5 ppm (J_{BP} of 49 Hz), exhibit such fine-coupling and can thus be assigned as arising from a phosphorus-adjacent cage boron and to the phosphorus-bonded borane, respectively.

DFT/GIAO computational investigations of the structures of **4a**$^-$, **5a**$^-$, **6a**$^-$, and **7a** yielded the optimized geometries **IVa**$^-$, **Va**$^-$, **VIa**$^-$, and **VIIa** (Figures 10 and 11b) having calculated ^{11}B, ^{13}C, and ^{31}P NMR chemical shifts (Table 1) in good agreement with the experimental values. The calculations also correctly assign the ^{11}B NMR resonances that exhibit J_{PB} coupling to borons directly bonded to the phosphorus. Consistent with the fact that the *endo*-hydrogen in **2a** undergoes reversible deprotonation/protonation, the DFT/GIAO calculations confirm that the O, S, BH_3, and Br-substituents are bonded at the phosphorus endo position. While the calculated ^{31}P NMR shifts for **4a**$^-$, **5a**$^-$, and **6a**$^-$ are in reasonable agreement with their experimentally determined chemical shift values, the difference between the calculated (58.6 ppm) and observed (16.3 ppm) shifts of the phosphorus resonance in **7a** is much larger. This

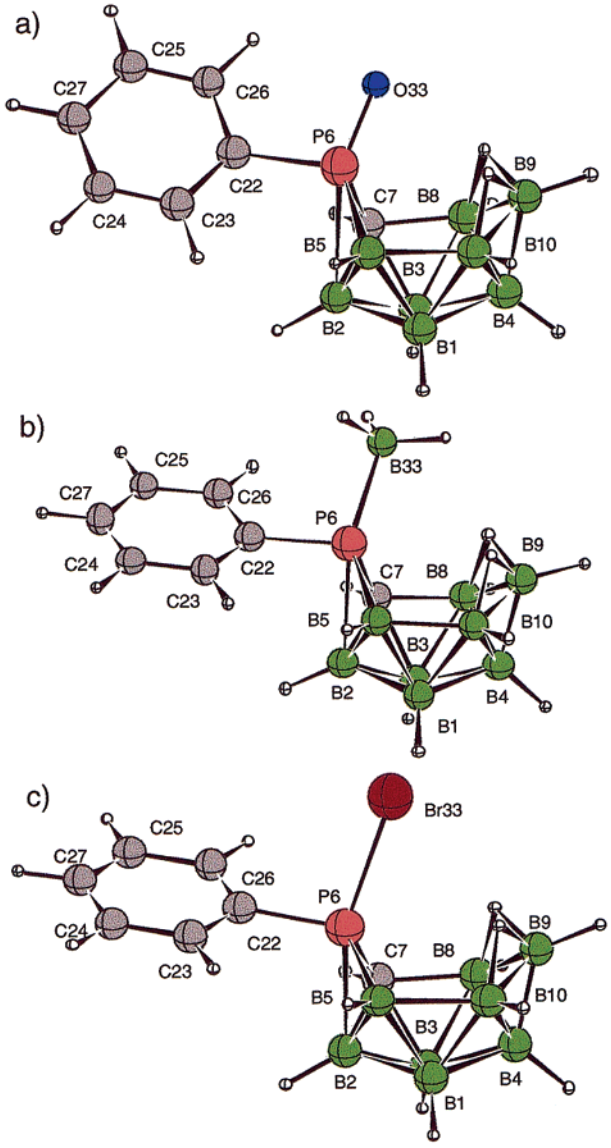

Figure 10. DFT optimized geometries for (a) **IVa**$^-$, selected calculated bond distances (Å) and angles (°): P6−O33, 1.520; P6−B2, 2.318; P6−B5, 1.913; P6−C7, 1.874, C7−B8, 1.675; B8−B9, 1.805; B9−B10, 1.824; B5−B10, 1.841; P6−C22, 1.855; C22−P6−B2, 95.0; C22−P6−C7, 105.2; C22−P6−B5, 113.1; C7−P6−B5, 89.4; B10−B9−B8, 101.1; O33−P6−C22, 105.3; O33−P6−C7, 114.9; O33−P6−B5, 126.7. (b) **VIa**$^-$, selected calculated bond distances (Å) and angles (°): P6−B33, 1.988; P6−B2, 2.284; P6−B5, 1.947; P6−C7, 1.878, C7−B8, 1.650; B8−B9, 1.813; B9−B10, 1.833; B5−B10, 1.803; P6−C22, 1.861; C22−P6−B2, 90.7; C22−P6−C7, 105.8; C22−P6−B5, 110.3; C7−B6−B5, 89.3; B10−B9−B8, 100.9; B33−P6−C22, 103.9; B33−P6−C7, 116.8; B33−P6−B5, 128.8. (c) **VIIa**, selected calculated bond distances (Å) and angles (°): P6−Br, 2.375; P6−B2, 2.170; P6−B5, 1.876; P6−C7, 1.806, C7−B8, 1.711; B8−B9, 1.801; B9−B10, 1.800; B5−B10, 1.893; P6−C22, 1.822; C22−P6−B2, 100.5; C22−P6−C7, 111.0; C22−P6−B5, 118.3; C7−P6−B5, 94.1; B10−B9−B8, 102.1; Br−P6−C22, 98.9; Br−P6−C7, 111.1; Br−P6−B5, 123.7.

discrepancy is most likely due to the limitation of the 6-311G* basis set to accurately model the larger bromine atom.

The structure of compound **PSH**$^+$**5a**$^-$ was further established by means of an X-ray crystallographic determination. As shown in the ORTEP plot in Figure 11a, the structure of the **5a**$^-$ anion retains the same framework as the parent compound **2a** in which the phosphorus and carbon atoms are in adjacent positions on the puckered six-membered open face of the arachno cage

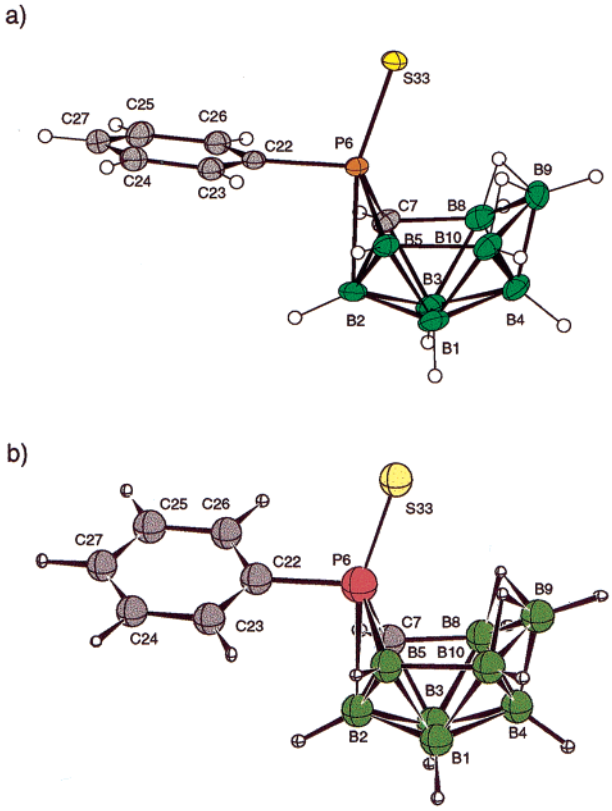

Figure 11. Comparison of the crystallographically determined structure of the *endo*-6-S-*exo*-6-(C_6H_5)-*arachno*-6,7-$PCB_8H_{11}^-$ anion in **PSH**$^+$**5a**$^-$ (a) with that of the DFT calculated geometry **Va**$^-$ (b). Selected bond distances (Å) and angles (°) in **5a**$^-$: P6−S33, 2.0042(10); P6−B2, 2.258-(3); P6−B5, 1.898(3); P6−C7, 1.829(3), C7−B8, 1.677(5); B8−B9, 1.807-(6); B9−B10, 1.810(6); B5−B10, 1.810(5); P6−C22, 1.817(3); C22−P6−B2, 91.84(13); C22−P6−C7, 106.43(13); C22−P6−B5, 110.47(14); C7−P6−B5, 90.89(14); B10−B9−B8, 100.9(2); S33−P6−C22, 105.48(8); S33−P6−C7, 117.46(10); S33−P6−B5, 124.69(11). Selected calculated bond distances (Å) and angles (°) for **Va**$^-$: P6−S33, 2.030; P6−B2, 2.308; P6−B5, 1.828; P6−C7, 1.871, C7−B8, 1.670; B8−B9, 1.802; B9−B10, 1.819; B5−B10, 1.834; P6−C22, 1.853; C22−P6−B2, 91.6; C22−P6−C7, 104.5; C22−P6−B5, 111.5; C7−P6−B5, 88.9; B10−B9−B8, 101.3; S33−P6−C22, 105.7; S33−P6−C7, 116.6; S33−P6−B5, 127.2.

framework. The bridging hydrogens again span the B8−B9 and B9−B10 edges. Consistent with the DFT calculations, the sulfur is found substituted at the endo position of the phosphorus. The observed P6−S bond distance of 2.0042(10) Å is substantially longer than that found for the P−S length in $SPPh_3$ (1.950(3) Å),[29] suggesting little multiple bond character to the P6−S bond in **5a**$^-$.

In conclusion, the studies discussed above have resulted in the development of rational high-yield routes to the first two examples of 10-vertex *arachno*- and *nido*-phosphamonocarbaboranes, *exo*-6-R-*arachno*-6,7-PCB_8H_{12} (**2**) and 6-R-*nido*-6,9-$PCB_8H_9^-$ (**3**$^-$), and should, therefore, now enable extensive investigations of the chemical properties of this new cluster class. However, of perhaps even greater significance, is the discovery of the unique donor properties of the *exo*-6-R-*arachno*-6,7-$PCB_8H_{11}^-$ (**2**$^-$) anion that emerged from the studies of its reactions (eqs 3−7) with Lewis acids. The insertion of electron-rich elements, such as phosphorus, into a boron cluster normally results in the formation of a compound having a formal lone pair of electrons associated with the heteroatom.[30] But,

(29) Codding, P. W.; Kerr, K. A. *Acta Crystallogr.* **1978**, *B34*, 3785−3787.

because of the extensive electron delocalization in polyhedral boron clusters, these heteroatom lone pairs are usually delocalized and have low Lewis basicity. As a result, they can neither be protonated nor form adducts with Lewis acids. Such was the case for $\mathbf{3}^-$, where it was found that it was not possible to protonate the anion even with concentrated H_2SO_4. In contrast, the reactions of the *exo*-6-R-*arachno*-6,7-$PCB_8H_{11}^-$ ($\mathbf{2}^-$) anion have demonstrated that it has a much different electronic distribution. Both the reversible deprotonation/reprotonation of **2** and the fact that $\mathbf{2a}^-$ reacts with O_2, S_8, BH_3, and Br_2 to yield the endo-substituted products $\mathbf{4a}^-$, $\mathbf{5a}^-$, $\mathbf{6a}^-$, and **7a** suggests that in $\mathbf{2}^-$ a lone pair of electrons is localized at the phosphorus endo position. This behavior appears to be unprecedented in phosphaborane chemistry. These studies further suggested to us that the $\mathbf{2}^-$ anions should be able to form adducts with an even wider variety of Lewis acids and, indeed, the following paper describes the syntheses and structural characterizations of a series of new types of metallaphosphamonocarbaborane complexes in which the metals adopt an unprecedented array of coordination geometries, including not only η^4, η^5, and η^6 metal-inserted bonding configurations, but also new types of sigma-donor *endo*-η^1 and *exo*-η^1 complexes in which the $\mathbf{2}^-$ anions are functioning, as has been previously observed for diphenylphosphidoboratabenzene $(PPh_2(BC_5H_5))^-$,[31] as an anionic equivalent of a PR_3 ligand.

Acknowledgment. This paper is dedicated to Professor Russell N. Grimes on the occasion of his retirement. We thank the National Science Foundation for support of this research.

Supporting Information Available: Tables listing Cartesian coordinates and energies for DFT-optimized geometries. X-ray crystallographic data for structure determinations of $\mathbf{PSH^+3a^-}$, $\mathbf{PSH^+3b^-}$, and $\mathbf{PSH^+5a^-}$ (CIF). This material is available free of charge via the Internet at http://pubs.acs.org.

JA020944J

(30) (a) Todd, L. J. In *Comprehensive Organometallic Chemistry*; Wilkinson, G., Stone, F. G. A., Abel, E. W., Eds.; Pergamon Press: New York, 1982; Vol. 1, pp 543−553. (b) Todd, L. J. In *Comprehensive Organometallic Chemistry*; Wilkinson, G., Stone, F. G. A., Abel, E. W., Housecroft, C. E., Eds.; Pergamon Press: New York, 1995; Vol. 1, pp 257−273. (c) Binder, H.; Hein, M. *Coord. Chem. Rev.* **1997**, *158*, 171−232.

(31) Hoic, D. A.; Davis, W. M.; Fu, G. C. *J. Am. Chem. Soc.* **1996**, *118*, 8176−8177.